

Di-jet production in $\gamma\gamma$ collisions at LEP2

DELPHI Collaboration

Abstract

The production of two high- p_T jets in the interactions of quasi-real photons in e^+e^- collisions at $\sqrt{s_{ee}}$ from 189 GeV to 209 GeV is studied with data corresponding to an integrated e^+e^- luminosity of 550 pb^{-1} . The jets reconstructed by the k_\perp -cluster algorithm are defined within the pseudo-rapidity range $-1 < \eta < 1$ and with jet transverse momentum, p_T , above 3 GeV/c. The differential di-jet cross-section is measured as a function of the mean transverse momentum $\overline{p_T}$ of the jets and is compared to perturbative QCD calculations.

(Accepted by Eur. Phys. J. C)

J.Abdallah²⁷, P.Abreu²⁴, W.Adam⁵⁶, P.Adzic¹³, T.Albrecht¹⁹, R.Aleman-Fernandez¹⁰, T.Allmendinger¹⁹, P.P.Allport²⁵, U.Amaldi³¹, N.Amapane⁴⁹, S.Amato⁵³, E.Anashkin³⁸, A.Andreazza³⁰, S.Andringa²⁴, N.Anjos²⁴, P.Antilogus²⁷, W-D.Apel¹⁹, Y.Arnoud¹⁶, S.Ask¹⁰, B.Asman⁴⁸, J.E.Augustin²⁷, A.Augustinus¹⁰, P.Baillon¹⁰, A.Ballestrero⁵⁰, P.Bambade²², R.Barbier²⁹, D.Bardin¹⁸, G.J.Barker⁵⁸, A.Baroncelli⁴¹, M.Battaglia¹⁰, M.Baubillier²⁷, K-H.Becks⁵⁹, M.Begalli⁸, A.Behrmann⁵⁹, E.Ben-Haim²², N.Benekos³⁴, A.Benvenuti⁶, C.Berat¹⁶, M.Berggren²⁷, D.Bertrand³, M.Besancon⁴², N.Besson⁴², D.Bloch¹¹, M.Blom³³, M.Bluj⁵⁷, M.Bonesini³¹, M.Boonekamp⁴², P.S.L.Booth^{†25}, G.Borisov²³, O.Botner⁵⁴, B.Bouquet²², T.J.V.Bowcock²⁵, I.Boyko¹⁸, M.Bracko⁴⁵, R.Brenner⁵⁴, E.Brodet³⁷, P.Bruckman²⁰, J.M.Brunet⁹, B.Buschbeck⁵⁶, P.Buschmann⁵⁹, M.Calvi³¹, T.Camporesi¹⁰, V.Canale⁴⁰, F.Carena¹⁰, N.Castro²⁴, F.Cavallo⁶, M.Chapkin⁴⁴, Ph.Charpentier¹⁰, P.Checchia³⁸, R.Chierici¹⁰, P.Chliapnikov⁴⁴, J.Chudoba¹⁰, S.U.Chung¹⁰, K.Cieslik²⁰, P.Collins¹⁰, R.Contri¹⁵, G.Cosme²², F.Cossutti⁵¹, M.J.Costa⁵⁵, D.Crennell³⁹, J.Cuevas³⁶, J.D'Hondt³, T.da Silva⁵³, W.Da Silva²⁷, G.Della Ricca⁵¹, A.De Angelis⁵², W.De Boer¹⁹, C.De Clercq³, B.De Lotto⁵², N.De Maria⁴⁹, A.De Min³⁸, L.de Paula⁵³, L.Di Ciaccio⁴⁰, A.Di Simone⁴¹, K.Doroba⁵⁷, J.Drees^{59,10}, G.Eigen⁵, T.Ekelof⁵⁴, M.Ellert⁵⁴, M.Elsing¹⁰, M.C.Espirito Santo²⁴, G.Fanourakis¹³, D.Fassouliotis^{13,4}, M.Feindt¹⁹, J.Fernandez⁴³, A.Ferrer⁵, F.Ferro¹⁵, U.Flammeyer⁵⁹, H.Foeth¹⁰, E.Fokitis³⁴, F.Fulda-Quenzer²², J.Fuster⁵⁵, M.Gandelman⁵³, C.Garcia⁵⁵, Ph.Gavillet¹⁰, E.Gaziz³⁴, R.Gokieli^{10,57}, B.Golob^{45,47}, G.Gomez-Ceballos⁴³, P.Goncalves²⁴, E.Graziani⁴¹, G.Grosdidier²², K.Grzelak⁵⁷, J.Guy³⁹, C.Haag¹⁹, A.Hallgren⁵⁴, K.Hamacher⁵⁹, K.Hamilton³⁷, S.Haug³⁵, F.Hauler¹⁹, V.Hedberg²⁸, M.Hennecke¹⁹, J.Hoffman⁵⁷, S-O.Holmgren⁴⁸, P.J.Holt¹⁰, M.A.Houlden²⁵, J.N.Jackson²⁵, G.Jarlskog²⁸, P.Jarry⁴², D.Jeans³⁷, E.K.Johansson⁴⁸, P.Jonsson²⁹, C.Joram¹⁰, L.Jungermann¹⁹, F.Kapusta²⁷, S.Katsanevas²⁹, E.Katsoufis³⁴, G.Kernel⁴⁵, B.P.Kersevan^{45,47}, U.Kerzel¹⁹, B.T.King²⁵, N.J.Kjaer¹⁰, P.Kluit³³, P.Kokkinias¹³, C.Kourkouvelis⁴, O.Kouznetsov¹⁸, Z.Krumstein¹⁸, M.Kucharczyk²⁰, J.Lamsa¹, G.Leder⁵⁶, F.Ledroit¹⁶, L.Leinonen⁴⁸, R.Leitner³², J.Lemone³, V.Lepeltier^{†22}, T.Lesiak²⁰, W.Liebig⁵⁹, D.Liko⁵⁶, A.Lipniacka⁴⁸, J.H.Lopes⁵³, J.M.Lopez³⁶, D.Loukas¹³, P.Lutz⁴², L.Lyons³⁷, J.MacNaughton⁵⁶, A.Malek⁵⁹, S.Maltezos³⁴, F.Mandl⁵⁶, J.Marco⁴³, R.Marco⁴³, B.Marechal⁵³, M.Margoni³⁸, J-C.Marin¹⁰, C.Mariotti¹⁰, A.Markou¹³, C.Martinez-Rivero⁴³, J.Masik¹⁴, N.Mastroiannopoulos¹³, F.Matorras⁴³, C.Matteuzzi³¹, F.Mazzucato³⁸, M.Mazzucato³⁸, R.Mc Nulty²⁵, C.Meroni³⁰, E.Migliore⁴⁹, W.Mitaroff⁵⁶, U.Mjoernmark²⁸, T.Moa⁴⁸, M.Moch¹⁹, K.Moenig^{10,12}, R.Monge¹⁵, J.Montenegro³³, D.Moraes⁵³, S.Moreno²⁴, P.Morettini¹⁵, U.Mueller⁵⁹, K.Muenich⁵⁹, M.Muldres³³, L.Mundim⁸, W.Murray³⁹, B.Muryn²¹, G.Myatt³⁷, T.Myklebust³⁵, M.Nassiakou¹³, F.Navarria⁶, K.Nawrocki⁵⁷, S.Nemecek¹⁴, R.Nicolaidou⁴², M.Nikolenko^{18,11}, A.Oblakowska-Mucha²¹, V.Obraztsov⁴⁴, A.Olshevski¹⁸, A.Onofre²⁴, R.Orava¹⁷, K.Osterberg¹⁷, A.Ouraou⁴², A.Oyanguren⁵⁵, M.Paganoni³¹, S.Paiano⁶, J.P.Palacios²⁵, H.Palka²⁰, Th.D.Papadopoulou³⁴, L.Pape¹⁰, C.Parkes²⁶, F.Parodi¹⁵, U.Parzefall¹⁰, A.Passerì⁴¹, O.Passon⁵⁹, L.Peralta²⁴, V.Perepelitsa⁵⁵, A.Perrotta⁶, A.Petrolini¹⁵, J.Piedra⁴³, L.Pieri⁴¹, F.Pierre⁴², M.Pimenta²⁴, E.Piotto¹⁰, T.Podobnik^{45,47}, V.Poireau¹⁰, M.E.Pol⁷, G.Polok²⁰, V.Pozdniakov¹⁸, N.Pukhaeva¹⁸, A.Pullia³¹, D.Radojicic³⁷, P.Rebecchi¹⁰, J.Rehn¹⁹, D.Reid³³, R.Reinhardt⁵⁹, P.Renton³⁷, F.Richard²², J.Ridky¹⁴, M.Rivero⁴³, D.Rodriguez⁴³, A.Romero⁴⁹, P.Ronchese³⁸, P.Roudeau²², T.Rovelli⁶, V.Ruhlmann-Kleider⁴², D.Ryabtchikov⁴⁴, A.Sadovsky¹⁸, L.Salmi¹⁷, J.Salt⁵⁵, C.Sander¹⁹, A.Savoy-Navarro²⁷, U.Schwickerath¹⁰, R.Sekulin³⁹, M.Siebel⁵⁹, A.Sisakian¹⁸, G.Smadja²⁹, O.Smirnova²⁸, A.Sokolov⁴⁴, A.Sopczak²³, R.Sosnowski⁵⁷, T.Spassov¹⁰, M.Stanitzki¹⁹, A.Stocchi²², J.Strauss⁵⁶, B.Stugu⁵, M.Szczekowski⁵⁷, M.Szeptycka⁵⁷, T.Szumlak²¹, T.Tabarelli³¹, F.Tegenfeldt⁵⁴, J.Timmermans³³, L.Tkatchev¹⁸, M.Tobin²⁵, S.Todorovova¹⁴, B.Tome²⁴, A.Tonazzo³¹, P.Tortosa⁵⁵, P.Travnicek¹⁴, D.Treille¹⁰, G.Tristram⁹, M.Trochimczuk⁵⁷, C.Troncon³⁰, M-L.Turluer⁴², I.A.Tyapkin¹⁸, S.Tzamarias¹³, V.Uvarov⁴⁴, G.Valenti⁶, P.Van Dam³³, J.Van Eldik¹⁰, N.van Remortel², I.Van Vulpen¹⁰, G.Vegni³⁰, F.Veloso²⁴, W.Venus³⁹, P.Verdier²⁹, Yu.L.Vertogradova¹⁸, V.Verzi⁴⁰, D.Vilanova⁴², L.Vitale⁵¹, V.Vrba¹⁴, H.Wahlen⁵⁹, A.J.Washbrook²⁵, C.Weiser¹⁹, D.Wicke¹⁰, J.Wickens³, G.Wilkinson³⁷, M.Winter¹¹, M.Witek²⁰, O.Yushchenko⁴⁴, A.Zalewska²⁰, P.Zalewski⁵⁷, D.Zavrtanik⁴⁶, V.Zhuravlov¹⁸, N.I.Zimin¹⁸, A.Zintchenko¹⁸, M.Zupan¹³

-
- ¹Department of Physics and Astronomy, Iowa State University, Ames IA 50011-3160, USA
- ²Physics Department, Universiteit Antwerpen, Universiteitsplein 1, B-2610 Antwerpen, Belgium
- ³IIHE, ULB-VUB, Pleinlaan 2, B-1050 Brussels, Belgium
- ⁴Physics Laboratory, University of Athens, Solonos Str. 104, GR-10680 Athens, Greece
- ⁵Department of Physics, University of Bergen, Allégaten 55, NO-5007 Bergen, Norway
- ⁶Dipartimento di Fisica, Università di Bologna and INFN, Via Irnerio 46, IT-40126 Bologna, Italy
- ⁷Centro Brasileiro de Pesquisas Físicas, rua Xavier Sigaud 150, BR-22290 Rio de Janeiro, Brazil
- ⁸Inst. de Física, Univ. Estadual do Rio de Janeiro, rua São Francisco Xavier 524, Rio de Janeiro, Brazil
- ⁹Collège de France, Lab. de Physique Corpusculaire, IN2P3-CNRS, FR-75231 Paris Cedex 05, France
- ¹⁰CERN, CH-1211 Geneva 23, Switzerland
- ¹¹Institut de Recherches Subatomiques, IN2P3 - CNRS/ULP - BP20, FR-67037 Strasbourg Cedex, France
- ¹²Now at DESY-Zeuthen, Platanenallee 6, D-15735 Zeuthen, Germany
- ¹³Institute of Nuclear Physics, N.C.S.R. Demokritos, P.O. Box 60228, GR-15310 Athens, Greece
- ¹⁴FZU, Inst. of Phys. of the C.A.S. High Energy Physics Division, Na Slovance 2, CZ-182 21, Praha 8, Czech Republic
- ¹⁵Dipartimento di Fisica, Università di Genova and INFN, Via Dodecaneso 33, IT-16146 Genova, Italy
- ¹⁶Institut des Sciences Nucléaires, IN2P3-CNRS, Université de Grenoble 1, FR-38026 Grenoble Cedex, France
- ¹⁷Helsinki Institute of Physics and Department of Physical Sciences, P.O. Box 64, FIN-00014 University of Helsinki, Finland
- ¹⁸Joint Institute for Nuclear Research, Dubna, Head Post Office, P.O. Box 79, RU-101 000 Moscow, Russian Federation
- ¹⁹Institut für Experimentelle Kernphysik, Universität Karlsruhe, Postfach 6980, DE-76128 Karlsruhe, Germany
- ²⁰Institute of Nuclear Physics PAN, Ul. Radzikowskiego 152, PL-31142 Krakow, Poland
- ²¹Faculty of Physics and Nuclear Techniques, University of Mining and Metallurgy, PL-30055 Krakow, Poland
- ²²LAL, Univ Paris-Sud, CNRS/IN2P3, Orsay, France
- ²³School of Physics and Chemistry, University of Lancaster, Lancaster LA1 4YB, UK
- ²⁴LIP, IST, FCUL - Av. Elias Garcia, 14-1º, PT-1000 Lisboa Codex, Portugal
- ²⁵Department of Physics, University of Liverpool, P.O. Box 147, Liverpool L69 3BX, UK
- ²⁶Dept. of Physics and Astronomy, Kelvin Building, University of Glasgow, Glasgow G12 8QQ, UK
- ²⁷LPNHE, IN2P3-CNRS, Univ. Paris VI et VII, Tour 33 (RdC), 4 place Jussieu, FR-75252 Paris Cedex 05, France
- ²⁸Department of Physics, University of Lund, Sölvegatan 14, SE-223 63 Lund, Sweden
- ²⁹Université Claude Bernard de Lyon, IPNL, IN2P3-CNRS, FR-69622 Villeurbanne Cedex, France
- ³⁰Dipartimento di Fisica, Università di Milano and INFN-MILANO, Via Celoria 16, IT-20133 Milan, Italy
- ³¹Dipartimento di Fisica, Univ. di Milano-Bicocca and INFN-MILANO, Piazza della Scienza 3, IT-20126 Milan, Italy
- ³²IPNP of MFF, Charles Univ., Areal MFF, V Holesovickach 2, CZ-180 00, Praha 8, Czech Republic
- ³³NIKHEF, Postbus 41882, NL-1009 DB Amsterdam, The Netherlands
- ³⁴National Technical University, Physics Department, Zografou Campus, GR-15773 Athens, Greece
- ³⁵Physics Department, University of Oslo, Blindern, NO-0316 Oslo, Norway
- ³⁶Dpto. Fisica, Univ. Oviedo, Avda. Calvo Sotelo s/n, ES-33007 Oviedo, Spain
- ³⁷Department of Physics, University of Oxford, Keble Road, Oxford OX1 3RH, UK
- ³⁸Dipartimento di Fisica, Università di Padova and INFN, Via Marzolo 8, IT-35131 Padua, Italy
- ³⁹Rutherford Appleton Laboratory, Chilton, Didcot OX11 0QX, UK
- ⁴⁰Dipartimento di Fisica, Università di Roma II and INFN, Tor Vergata, IT-00173 Rome, Italy
- ⁴¹Dipartimento di Fisica, Università di Roma III and INFN, Via della Vasca Navale 84, IT-00146 Rome, Italy
- ⁴²DAPNIA/Service de Physique des Particules, CEA-Saclay, FR-91191 Gif-sur-Yvette Cedex, France
- ⁴³Instituto de Física de Cantabria (CSIC-UC), Avda. los Castros s/n, ES-39006 Santander, Spain
- ⁴⁴Inst. for High Energy Physics, Serpukov P.O. Box 35, Protvino, (Moscow Region), Russian Federation
- ⁴⁵J. Stefan Institute, Jamova 39, SI-1000 Ljubljana, Slovenia
- ⁴⁶Laboratory for Astroparticle Physics, University of Nova Gorica, Kostanjevska 16a, SI-5000 Nova Gorica, Slovenia
- ⁴⁷Department of Physics, University of Ljubljana, SI-1000 Ljubljana, Slovenia
- ⁴⁸Fysikum, Stockholm University, Box 6730, SE-113 85 Stockholm, Sweden
- ⁴⁹Dipartimento di Fisica Sperimentale, Università di Torino and INFN, Via P. Giuria 1, IT-10125 Turin, Italy
- ⁵⁰INFN, Sezione di Torino and Dipartimento di Fisica Teorica, Università di Torino, Via Giuria 1, IT-10125 Turin, Italy
- ⁵¹Dipartimento di Fisica, Università di Trieste and INFN, Via A. Valerio 2, IT-34127 Trieste, Italy
- ⁵²Istituto di Fisica, Università di Udine and INFN, IT-33100 Udine, Italy
- ⁵³Univ. Federal do Rio de Janeiro, C.P. 68528 Cidade Univ., Ilha do Fundão BR-21945-970 Rio de Janeiro, Brazil
- ⁵⁴Department of Radiation Sciences, University of Uppsala, P.O. Box 535, SE-751 21 Uppsala, Sweden
- ⁵⁵IFIC, Valencia-CSIC, and D.F.A.M.N., U. de Valencia, Avda. Dr. Moliner 50, ES-46100 Burjassot (Valencia), Spain
- ⁵⁶Institut für Hochenergiephysik, Österr. Akad. d. Wissensch., Nikolsdorfergasse 18, AT-1050 Vienna, Austria
- ⁵⁷Inst. Nuclear Studies and University of Warsaw, Ul. Hoza 69, PL-00681 Warsaw, Poland
- ⁵⁸Now at University of Warwick, Coventry CV4 7AL, UK
- ⁵⁹Fachbereich Physik, University of Wuppertal, Postfach 100 127, DE-42097 Wuppertal, Germany
- † deceased

1 Introduction

This paper presents the results of a study of di-jet events produced in two-photon collisions in the anti-tagged mode, i.e. when both scattered electrons¹ escape detection. Large p_T processes involving quasi-real photons are sensitive to both, quark and gluon, components of the resolved photons. Thus, the analysis of high- p_T jet production complements the studies of the deep-inelastic structure function of a quasi-real photon which probe the quark distribution. Considered together, they allow the parton density function of the photon to be determined. The perturbative QCD scale of the hard interactions is provided by the jet transverse energy to be used in the calculations. Available leading and next-to-leading order calculations [1] can be tested with the large samples of LEP-2 data. The present analysis adds new results to those obtained by other LEP experiments [2,3].

Gamma-gamma collisions exhibit a behavior typical of hadron-hadron interactions, i.e. the centre-of-mass frame of the hard scattered partons is moving in the $\gamma\gamma$ centre-of-mass frame. The k_\perp -cluster algorithm [4–6], invariant under boosts along the beam axis, is used. The variables adopted for the jet analysis are the transverse momentum p_T , the azimuthal angle ϕ and the pseudo-rapidity $\eta = -\ln(\tan(\theta/2))$ of the particle(jet)².

Hadron production in the collisions of quasi-real photons is described by the set of processes illustrated in Fig. 1. The interaction of bare photons (the direct term) is described by the Born-box diagram within the quark-parton model (QPM). If one or both photons are resolved into a partonic structure, the process is termed single- or double-resolved, respectively. A part of the double-resolved interactions with both photons resolved into a bound quark-pair system is described by the vector dominance model (VDM). The relative contribution of the different components depends on the kinematic regime. The present study involves such a 3-component model in order to describe the data and to correct on the experimental effects and then to compare the data with leading order (LO) and next-to-leading order (NLO) QCD calculations.

An important issue is the expected difference in topology. Almost all hadrons produced in QPM-like events should belong to two hard-jets, while two jets in events with resolved photons are accompanied by remnant jet(s). The variables sensitive to such a difference are [7]

$$x_\gamma^+ = \frac{\sum_{\text{jets}} (E_{\text{jet}} + p_{z,\text{jet}})}{\sum_{\text{part}} (E_{\text{part}} + p_{z,\text{part}})} \quad \text{and} \quad x_\gamma^- = \frac{\sum_{\text{jets}} (E_{\text{jet}} - p_{z,\text{jet}})}{\sum_{\text{part}} (E_{\text{part}} - p_{z,\text{part}})},$$

where ‘part’ corresponds to all detected particles and E_{jet} and $p_{z,\text{jet}}$ are the two hard-jets energy and the component of jet momentum along the z-axis, respectively. These variables represent the respective fractions of the γ momenta relevant to the hard interaction. The photons in the QPM-like events participate in the interaction entirely and both x_γ^+ and x_γ^- should be equal to unity, while the presence of a remnant jet (single-resolved photon) shifts x_γ^+ or x_γ^- toward some lower values. In the double-resolved case, both variables are far from unity.

Experimental details are discussed in Section 2. Section 3 presents the analysis of the data which are compared to the leading and next-to-leading order QCD calculations [1]. Results and conclusions are given in Section 4.

¹Throughout this paper, electron stands for electron and positron.

²The origin of the DELPHI reference system is at the centre of the detector. The z-axis is parallel to the e^- beam, the x-axis points horizontally to the centre of the LEP ring and the y-axis points vertically upwards. The coordinates R, ϕ, z form a cylindrical coordinate system and θ is the polar angle with respect to the z-axis.

2 Detector and Data

The DELPHI apparatus and performance are described in detail in ref. [8,9].

Charged particles are detected in the tracking system containing a 3-layer silicon Vertex Detector, the Inner Detector, the Time Projection Chamber and the Outer Detector. The Forward Chambers extend the acceptance into the forward region. The tracking detectors are located inside the superconducting solenoid providing a uniform magnetic field of 1.23 T parallel to the axis of the colliding e^+/e^- beams. The combined momentum resolution provided by the tracking system is of the order of a few per-mille in the momentum range of the present study.

Photons are detected in the electromagnetic calorimeters - High density Projection Chamber in the barrel region and the Forward Electro-Magnetic Calorimeter in the end-caps with polar angle coverages of $(40^\circ - 140^\circ)$ and $(9^\circ - 35^\circ, 145^\circ - 171^\circ)$, respectively.

Jets are reconstructed from two kinds of detected objects - charged particles and photons.

The events of interest are quite energetic and the multiplicity of final state particles is large. The events are triggered by several components of the DELPHI trigger system [10] and the resulting efficiency is estimated to be equal to unity.

The data used for this analysis have been collected by the DELPHI detector at LEP at an e^+e^- centre-of-mass energy ($\sqrt{s_{ee}}$) from 189 GeV to 209 GeV and correspond to an integrated e^+e^- luminosity of 550 pb^{-1} .

2.1 Data selection

The following criteria are applied to select the data sample.

- **Multihadron event selection.**

Each event should contain at least 5 charged particles. A charged particle is counted if its momentum is greater than 0.2 GeV/c, the polar angle is within the interval from 20° to 160° , the relative momentum error is less than 100% and the impact parameters are smaller than 4 cm in $R\phi$ and 10 cm in z .

- **Background suppression.**

The invariant mass of the system calculated from the charged particles (assuming them to be pions) and the photons (detected in the electromagnetic calorimeters) should be below $35 \text{ GeV}/c^2$. The energy threshold for an electromagnetic calorimeter cluster is set to 0.5 GeV. The total transverse momentum $|\sum(\vec{p}_T)|$ should be below $30 \text{ GeV}/c$. These criteria suppress events coming from e^+e^- annihilation and they set upper limits (see below) for jet transverse momentum.

- **Anti-tagging condition.**

There should be no clusters in the luminosity monitor STIC (which covers the region from 29 mrad to 185 mrad in the polar angle) with energy greater than 25 GeV (anti-tagging condition). This ensures the photons to be quasi-real.

- **Di-jet event selection.**

Jets are reconstructed by the k_\perp -cluster algorithm, implemented in the KTCLUS program [6]. It operates with objects (at generator level they may be either particles or partons) and tries to unite them into a jet in a recursive way. The following variables are calculated for each object i and a pair of objects i and j :

$$d_i = E_{T,i}^2 \text{ and } d_{ij} = \min(d_i, d_j)[(\eta_i - \eta_j)^2 + (\phi_i - \phi_j)^2]/R^2,$$

where the transverse energy $E_{T,i}$ is calculated with pion mass assumption for a charged particle and zero mass for a photon, R is usually set to unity. If the smallest

value (d_{min}) of any d in this sample is the d_{ij} value of a pair (i, j) , then these two objects are joined into a new object and its E_T, ϕ and η are recalculated. Otherwise, if the smallest value in the sample is the d_i value of an object i , the corresponding object is not mergeable and it is moved from the object list to the jet list. The procedure continues until there are no more objects. The pseudo-rapidity η of exactly two jets must be in the range $-1 < \eta < 1$ and their transverse momenta, p_T , above 3 GeV/c. Besides these two hard process jets, the event may contain one or more jets outside the pseudo-rapidity and p_T domain mentioned above. They are termed ‘remnant’ jets. The choice of the kinematic limits is conditioned by the desire to suppress soft $\gamma\gamma$ interactions and to keep hard process jets within the DELPHI acceptance. The cut on jet p_T should not be too large since, besides decreasing the measurement accuracy, it reduces the contribution coming from events with resolved photons. The extension of the η domain results in an increase of threshold effects, since some of the produced jet particles are outside the detector acceptance and the efficiency of the jet reconstruction is decreased.

An additional cut on the mean jets transverse momentum $\overline{p_T} > 4$ GeV/c allows a p_T asymmetry of the reconstructed jets. If such a cut is applied symmetrically to each of the two jets, the QCD calculations of some variables are unstable [1].

The above criteria select a data sample of 5147 events. The data are corrected for detector inefficiency and acceptance effects with a leading-order (LO) Monte Carlo simulation described below. LO simulation is also used for the estimation of the soft processes accompanying the hard-initiated jets and for taking into account the influence of hadronisation.

2.2 Monte Carlo simulation and background estimation

The Monte Carlo generator PYTHIA (version 6.205) [11] is used for the simulation of hadron production in $\gamma\gamma$ interactions. The program contains an interface to an external library of parton density functions (PDF) for the photons [12]. The default SaS1D [13] PDF is taken. The soft underlying events are modeled through multiple parton interactions (MIA) of several parton pairs within the same event. An event with both photons resolved may contain, besides hard initiated jets and the corresponding remnant jets, such an additional MIA contribution.

The simulated sample is approximately 4 times larger than the data sample.

The main background process ($e^+e^- \rightarrow$ hadrons) is simulated by the KK2f event generator (version 4.14) [14]. The expected number of these background events in the selected data sample is estimated to (500 ± 5) events. The contamination of τ pairs produced in two-photon interactions is evaluated as (43 ± 3) events, using the BDKRC program [15]. The background of τ pairs produced in e^+e^- annihilation is negligible. The events with W, Z bosons contribute (38 ± 4) events.

Note that the mentioned background sources (they will be referred to as ‘non- $\gamma\gamma$ ’ background) are only a part of the total background. Additional sources will be discussed later in Section 3.2.

3 Analysis

The entire (x_γ^+, x_γ^-) -space can be split into four quadrants (Fig. 2) by x_γ equal to 0.85. The chosen value of x_γ selects approximately equal statistics in the different domains.

One can define three kinematic regions: the first - x_γ^+ and x_γ^- greater than 0.85 (the region is termed as ‘Dir’ domain), the second - when both values are below 0.85 (double-resolved domain, ‘DR’) and the third region - when one variable is below 0.85 while the other is above it (single-resolved, ‘SR’).

Figure 3 shows the total energy outside the reconstructed jets (E_{out}) in comparison with the model expectation. The contributions of different parts of the model are also presented in the figure.

The ‘Dir’ domain (Fig. 3b) is mostly populated by QPM-like events (94%), the contribution of the double-resolved subprocesses to the ‘DR’ domain (Fig. 3d) is around 54%, while the ‘SR’ domain (Fig. 3c) contains all three types in nearly equal parts. It is seen that the model does not describe the data in the parts of the (x_γ^+, x_γ^-) -space where the contribution of the resolved processes is essential. It is also clear that a simple one-parameter renormalization of the model as a whole as done in previous publications [2,3] is not adequate since its components have to be tuned separately with different factors. This renormalization is a new approach to the analysis of jets produced in $\gamma\gamma$ collisions.

A 3-parameters fit of the data is performed simultaneously on the following distributions: E_{out} (Fig. 3), the transverse momentum balance ($|\sum \vec{p}_{i,T}|$) (not shown) and the total invariant mass W of the detected particles (not shown). The distributions are fitted in each (x_γ^+, x_γ^-) -domain. The obtained parameters (scale factors α for each model component) are $\alpha_{qpm} = (0.86 \pm 0.02)$, $\alpha_{s-res} = (1.49 \pm 0.09)$ and $\alpha_{d-res} = (1.93 \pm 0.05)$.

Figure 4 presents the background-subtracted data compared to the $\gamma\gamma$ simulation (with scaling factors applied) for the variables which were not involved in the fit. The data are in good agreement with the simulation. The Monte Carlo set, scaled according to the fit parameters, consists of 33% QPM-like events, 23% single-resolved and 44% double-resolved events. Double-resolved events are subdivided into contributions ‘no-MIA’ (75%) and ‘with-MIA’ (25%).

3.1 Multiple parton interactions

As already mentioned the modeling of the double-resolved events includes the so-called multiple parton interactions (MIA) [11]. Since the resolved photons are composite objects consisting of many partons, it is assumed that different pairwise interactions may take place during one $\gamma\gamma$ collision. It has been shown that the inclusion of MIA improves the description of the data [16]. The amount of MIA in PYTHIA is determined by a cutoff parameter on the parton transverse momentum. The default value of 1.6 GeV/c is used. MIA influence the model predictions in two ways. The first is the case when the hard initiated jets satisfy the selection criteria and MIA systematically increase the jet transverse energy. The second way is when the hard process alone does not provide two jets passing the selection criteria but combined with MIA initiated particles the event is selected. The MIA contribution in this case is to the background and it has to be estimated and subtracted from the data according to the model expectation. For this purpose PYTHIA is run in the mode with MIA switched off. It is found that 27% of the double-resolved $\gamma\gamma$ interactions with MIA contributions would not pass the di-jet selection criteria if MIA were absent. Note that the double-resolved part of the model is fitted in a coherent way, i.e. without splitting it into subsamples with-MIA and without it.

Summarizing the MIA influence, the model predicts the background coming from MIA as 7% (3%) of the double-resolved part (the total model prediction). On the other hand 18% of the double-resolved events are affected by MIA via the increase of the jet transverse

momentum. The absolute value of the background coming from the MIA contribution is estimated as (131 ± 7) events. The importance of the 3-parameter fit performed has to be emphasized since the evaluation of the background is done by using the scale factors obtained.

3.2 Hadronisation corrections, acceptance and background subtraction

The theoretical predictions have to be transformed from the parton level to the level at which particles are produced in the $\gamma\gamma$ interaction vertex - the particle level ('hadronisation corrections'). The Monte Carlo partons are considered in leading-order and are not identical to the NLO partons in the theoretical calculations. The corrections have been calculated using the PYTHIA program. The distribution of the mean transverse momentum of the jets $\overline{p_T}$ (difference of jet pseudo-rapidities $|\Delta\eta|$) obtained with the k_{\perp} -cluster algorithm at the parton level, is divided by the distribution obtained after hadronisation. The resulting 'hadronisation corrections' are shown in Fig. 5. They reach 60% value at smallest p_T and decrease to 30% for higher transverse momentum.

The next step is to transform the data from the level of the detected particles to the hadrons produced in $\gamma\gamma$ interactions in order to take the detector acceptance into account. The detector acceptance enters in two ways - either some events do not satisfy the selection and thus they are lost or the observed distributions in the selected events are distorted. Bin-by-bin corrections are used. Figure 6 illustrates the detector efficiency as a function of $\overline{p_T}$ (the dip in the middle of the distribution is caused by limited statistics of the simulation) and $|\Delta\eta|$.

Note that these corrections apply to two-jet events. The first correction transfers the two-jet calculations carried out at the parton level to model expectations at the level of the produced particles. The acceptance has been calculated both at the produced and detected particle levels for the two-jet events. That is why the following and last source of background ('non2-to-2 jets') should be taken into account. Some events are reconstructed with two jets because undetected particles change the event topology, but they do not have two jets at the production level. This kind of background is estimated as (893 ± 13) events and it becomes the largest source of background for the di-jet studies.

4 Results and conclusions

Figures 7(a-b) show the $\overline{p_T}$ and $|\Delta\eta|$ data distributions compared to the total simulation. All sources of the background mentioned above are given there as well.

The data are bin-to-bin corrected for the acceptance and, applying the integrated luminosity of LEP corresponding to the data, the total di-jet cross-section is measured to be 17.8 ± 0.6 pb for jets within the pseudo-rapidity range of $-1 < \eta < 1$ and for a jet transverse momentum p_T above 3 GeV/c. The statistical and systematic uncertainties (approximately of equal size) are added in quadrature. The systematic uncertainty includes the errors of the fit mentioned above, the uncertainty coming from MIA handling and the background estimations. The model expectations are 20.5 ± 0.1 pb and 18.1 ± 0.6 pb for the calculations carried out in the leading and next-to-leading order, respectively. The differential cross-sections are obtained with bin-by-bin corrections for the detector efficiency (Fig. 6) for the data and with 'hadronisation corrections' (Fig. 5) applied to the theoretical calculations. The obtained cross-sections are shown in Fig. 8 and compared to

the predictions mentioned above (the NLO calculations done with Monte Carlo method have sizable uncertainties which are shown on the plots). Numerical results are presented in Table 1 as a function of $\overline{p_T}$ and in Table 2 as a function of $|\Delta\eta|$. The errors include statistical and systematic uncertainties added in quadrature.

Since we scaled the contribution of QPM-like events (‘direct’ term) and this part is well calculable, it seems interesting to compare the scaled distributions to the results of calculations carried out in the leading and next-to-leading orders. The results are presented in Fig. 9. The scaled ‘direct’ term is only around 10% below NLO calculations; the main difference comes from the small $\overline{p_T}$ domain, while there is good agreement with NLO calculations for $\overline{p_T}$ greater than 4.5 GeV/c.

In conclusion, the production of two high- p_T jets in the interactions of quasi-real photons is studied with the DELPHI data taken at LEP-2 with an integrated e^+e^- luminosity of 550 pb⁻¹. The jets reconstructed by the k_\perp -cluster algorithm are defined within the pseudo-rapidity range of $-1 < \eta < 1$ and for a jet transverse momentum p_T above 3 GeV/c. The total and differential di-jet cross-sections are measured for a mean jet momentum $\overline{p_T}$ from 4 GeV/c to 14 GeV/c. The total cross-section agrees with the next-to-leading order perturbative QCD calculation within the experimental uncertainties and is 18% below the calculation carried out in the leading order. The measured differential di-jet cross-section is also found to be in good agreement with NLO QCD predictions [1] and complements results obtained by other LEP experiments [2,3].

Acknowledgements

We are greatly indebted to our technical collaborators, to the members of the CERN-SL Division for the excellent performance of the LEP collider, and to the funding agencies for their support in building and operating the DELPHI detector.

We acknowledge in particular the support of

Austrian Federal Ministry of Education, Science and Culture, GZ 616.364/2-III/2a/98,
FNRS-FWO, Flanders Institute to encourage scientific and technological research in the industry (IWT) and Belgian Federal Office for Scientific, Technical and Cultural affairs (OSTC), Belgium,

FINEP, CNPq, CAPES, FUJB and FAPERJ, Brazil,

Ministry of Education of the Czech Republic, project LC527,

Academy of Sciences of the Czech Republic, project AV0Z10100502,

Commission of the European Communities (DG XII),

Direction des Sciences de la Matière, CEA, France,

Bundesministerium für Bildung, Wissenschaft, Forschung und Technologie, Germany,

General Secretariat for Research and Technology, Greece,

National Science Foundation (NWO) and Foundation for Research on Matter (FOM),

The Netherlands,

Norwegian Research Council,

State Committee for Scientific Research, Poland, SPUB-M/CERN/PO3/DZ296/2000,

SPUB-M/CERN/PO3/DZ297/2000, 2P03B 104 19 and 2P03B 69 23(2002-2004),

FCT - Fundação para a Ciência e Tecnologia, Portugal,

Vedecka grantova agentura MS SR, Slovakia, Nr. 95/5195/134,

Ministry of Science and Technology of the Republic of Slovenia,

CICYT, Spain, AEN99-0950 and AEN99-0761,

The Swedish Research Council,

The Science and Technology Facilities Council, UK,

Department of Energy, USA, DE-FG02-01ER41155,
EEC RTN contract HPRN-CT-00292-2002.

References

- [1] M. Klasen and G. Kramer, Phys. Lett. **B366** (1996) 385;
M. Klasen, private communication.
- [2] OPAL Collab., G. Abbiendi *et al.*, Eur. Phys. J. **C31** (2003) 307.
- [3] L3 Collab., P. Achard *et al.*, Phys. Lett. **B602** (2004) 157.
- [4] S.D. Ellis and D.E. Soper, Phys. Rev. **D48** (1993) 3160.
- [5] S. Catani *et al.*, Nucl. Phys. **B406** (1993) 187.
- [6] M. Seymour, code source <http://hepwww.rl.ac.uk/theory/seymour/ktclus>.
- [7] L. Lönnblad and M. Seymour (conveners), section ‘ $\gamma\gamma$ event generators’ in ‘Physics at LEP2’, ed. G. Altarelli, T. Sjöstrand and F. Zwirner, CERN 96-01 (1996), volume 2, 204.
- [8] DELPHI Collab., P. Aarnio *et al.*, Nucl. Instr. & Meth. **A303** (1991) 233.
- [9] DELPHI Collab., P. Abreu *et al.*, Nucl. Instr. & Meth. **A378** (1996) 57.
- [10] DELPHI Trigger Group, A. Augustinus *et al.*, Nucl. Instr. & Meth. **A515** (2003) 782.
- [11] T. Sjöstrand, Comput. Phys. Commun. **82** (1994) 74.
- [12] H. Plochow-Besch, Int. J. Mod. Phys. **A10** (1995) 2901.
- [13] G. A. Schuler and T. Sjöstrand, Z. Phys. **C68** (1995) 607.
- [14] S. Jadach, B. F. L. Ward and Z. Was, Comput. Phys. Commun. **130** (2000) 260.
- [15] F. Berends, P. Daverveldt and R. Kleiss, Comput. Phys. Commun. **40** (1986) 271, 285 and 309.
- [16] H1 Collab., S. Aid *et al.*, Z. Phys. **C70** (1996) 17.

$p_{T,mean}$	$\sigma_{measured,total}$ (pb/GeV)	σ_{LO} (pb/GeV)	σ_{NLO} (pb/GeV)
4.0-4.5	9.59 ± 0.53	11.59 ± 0.13	9.75 ± 0.85
4.5-5.0	6.71 ± 0.41	7.61 ± 0.10	6.71 ± 0.53
5.0-5.5	4.56 ± 0.33	5.24 ± 0.07	4.49 ± 0.27
5.5-6.0	3.06 ± 0.26	3.86 ± 0.06	3.49 ± 0.19
6.0-7.0	2.19 ± 0.16	2.46 ± 0.04	2.28 ± 0.12
7.0-8.0	1.17 ± 0.12	1.40 ± 0.03	1.28 ± 0.08
8.0-9.0	0.88 ± 0.12	0.88 ± 0.02	0.79 ± 0.06
9.0-10.0	0.71 ± 0.11	0.61 ± 0.02	0.58 ± 0.05
10.0-12.0	0.31 ± 0.05	0.33 ± 0.01	0.31 ± 0.03
12.0-14.0	0.11 ± 0.03	0.18 ± 0.01	0.16 ± 0.03

Table 1: Measured cross-section of di-jet production in quasi-real $\gamma\gamma$ interactions as a function of $\overline{p_T}$ together with leading order and next-to-leading order calculations [1].

$ \Delta\eta $	$\sigma_{measured,total}$ (pb)	σ_{LO} (pb)	σ_{NLO} (pb)
0.-0.2	3.50 ± 0.21	4.23 ± 0.05	3.44 ± 0.25
0.2-0.4	2.96 ± 0.18	3.66 ± 0.05	2.76 ± 0.20
0.4-0.6	2.54 ± 0.18	3.31 ± 0.04	3.32 ± 0.25
0.6-0.8	2.67 ± 0.19	2.81 ± 0.04	2.36 ± 0.19
0.8-1.0	2.09 ± 0.17	2.35 ± 0.04	2.20 ± 0.24
1.0-1.2	1.78 ± 0.16	1.87 ± 0.03	1.84 ± 0.20
1.2-1.4	1.39 ± 0.14	1.38 ± 0.03	1.28 ± 0.13
1.4-1.6	0.67 ± 0.11	0.95 ± 0.02	0.80 ± 0.09
1.6-1.8	0.29 ± 0.12	0.54 ± 0.02	0.63 ± 0.09
1.8-2.0	0.29 ± 0.11	0.16 ± 0.02	0.09 ± 0.04

Table 2: Measured cross-section of di-jet production in quasi-real $\gamma\gamma$ interactions as a function of $|\Delta\eta|$ together with leading order and next-to-leading order calculations [1].

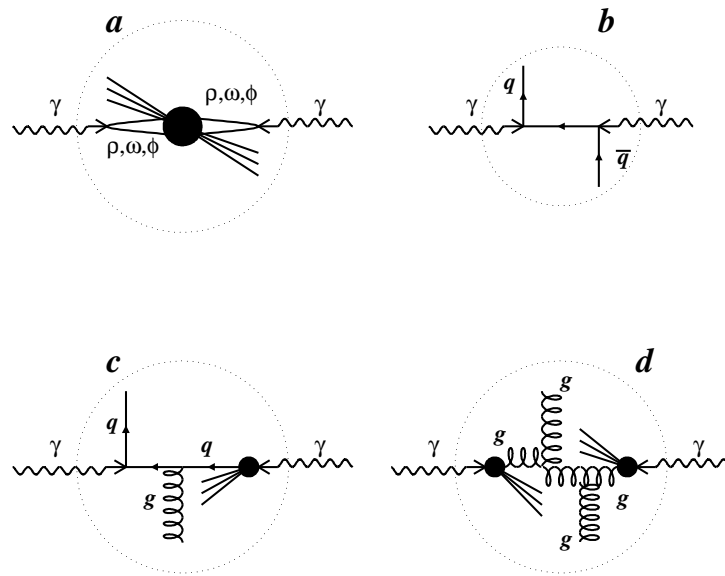


Figure 1: Main diagrams corresponding to the hadron production in $\gamma\gamma$ interactions via vector meson interactions (VDM-like, a), point-like interactions (QPM-like, b) and with one (c) or both (d) photons resolved into partons.

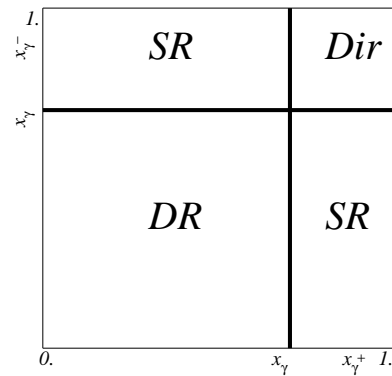


Figure 2: (x_γ^+, x_γ^-) -space divided by x_γ into four domains ('Dir', 'SR' and 'DR' notations are introduced in section 3).

DELPHI

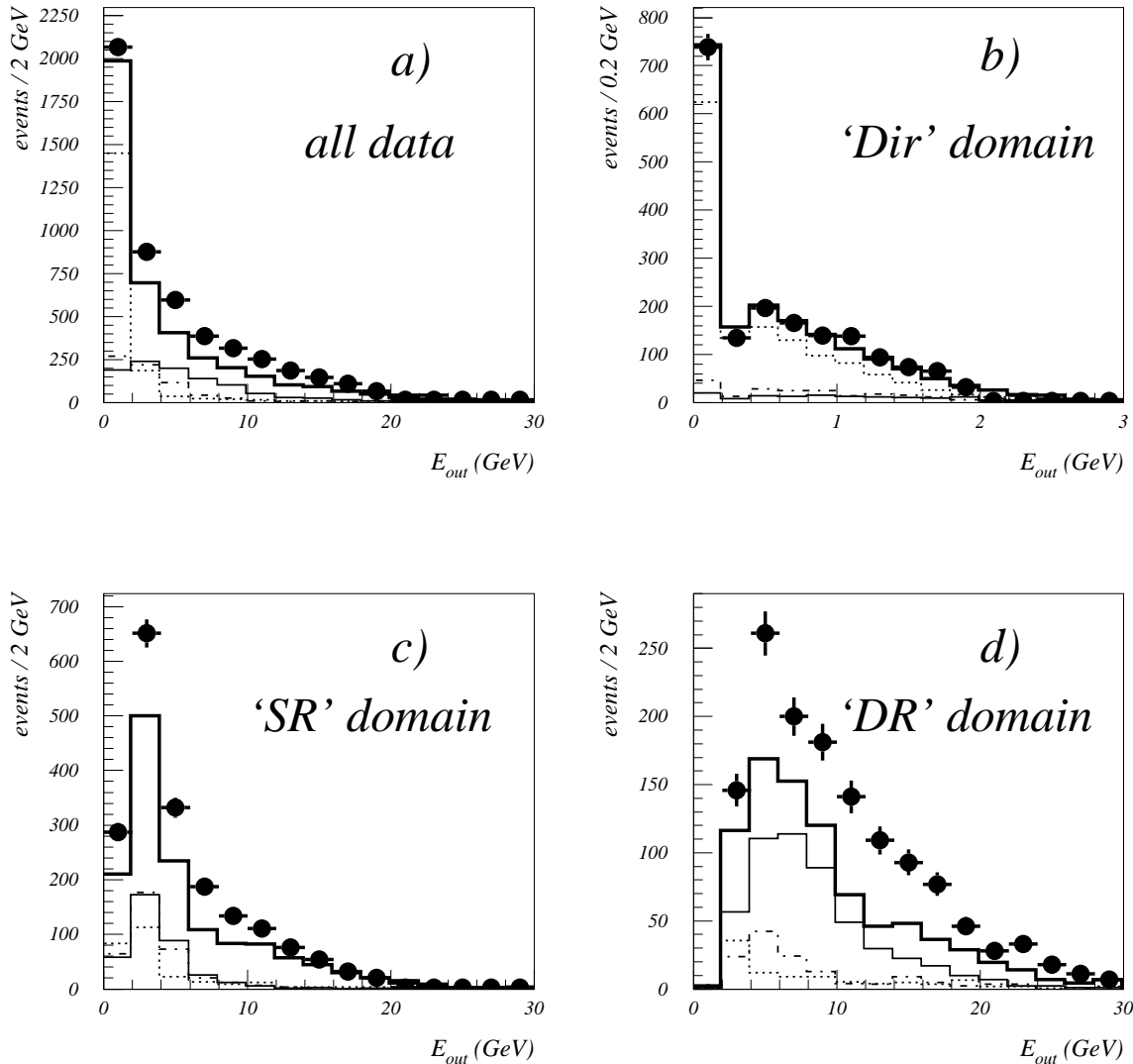


Figure 3: Comparison of the total energy outside the reconstructed jets E_{out} with the simulation for the selected data (a), and data in the phase-space domains ‘Dir’ (b), ‘SR’ (c) and ‘DR’ (d), described in section 3 of the text. The thick solid histograms correspond to the sum of the di-jet $\gamma\gamma$ interactions as predicted by PYTHIA and the background processes. The contributions of different $\gamma\gamma$ subprocesses are shown by dotted (QPM term), dashed-dotted (single-resolved) and thin solid (double-resolved) histograms.

DELPHI

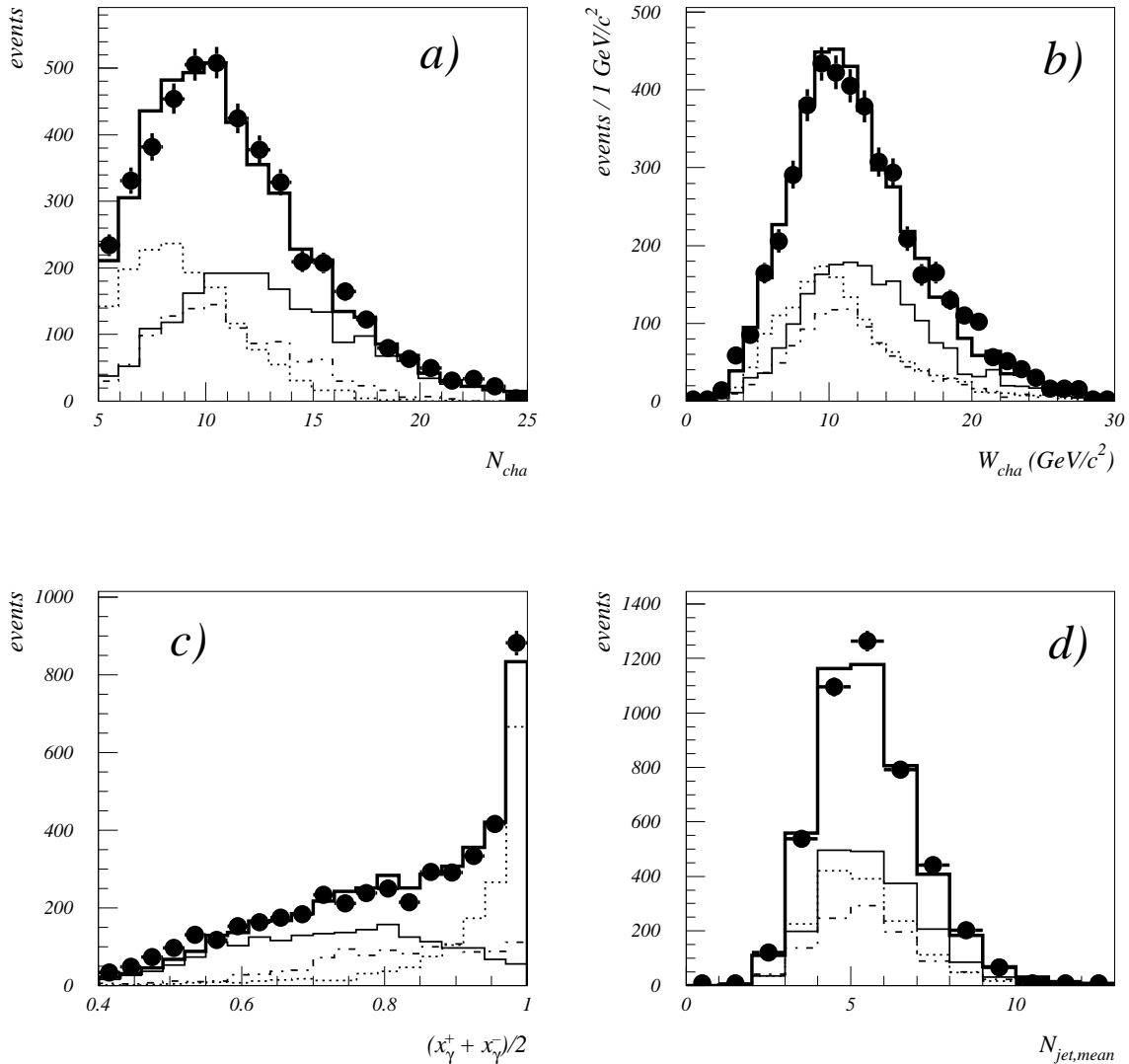


Figure 4: Comparison of the background subtracted data with the simulation after the fit for the charged multiplicity (a), the invariant mass calculated with the charged particles only (b), $(x_{\gamma}^+ + x_{\gamma}^-)/2$ (c) and the mean number of particles in the reconstructed jets (d). The simulation (thick solid histograms) sums all three model components scaled with the factors given in the text. The contributions of $\gamma\gamma$ subprocesses are shown by dotted (QPM term), dashed-dotted (single-resolved) and thin solid (double-resolved) histograms.

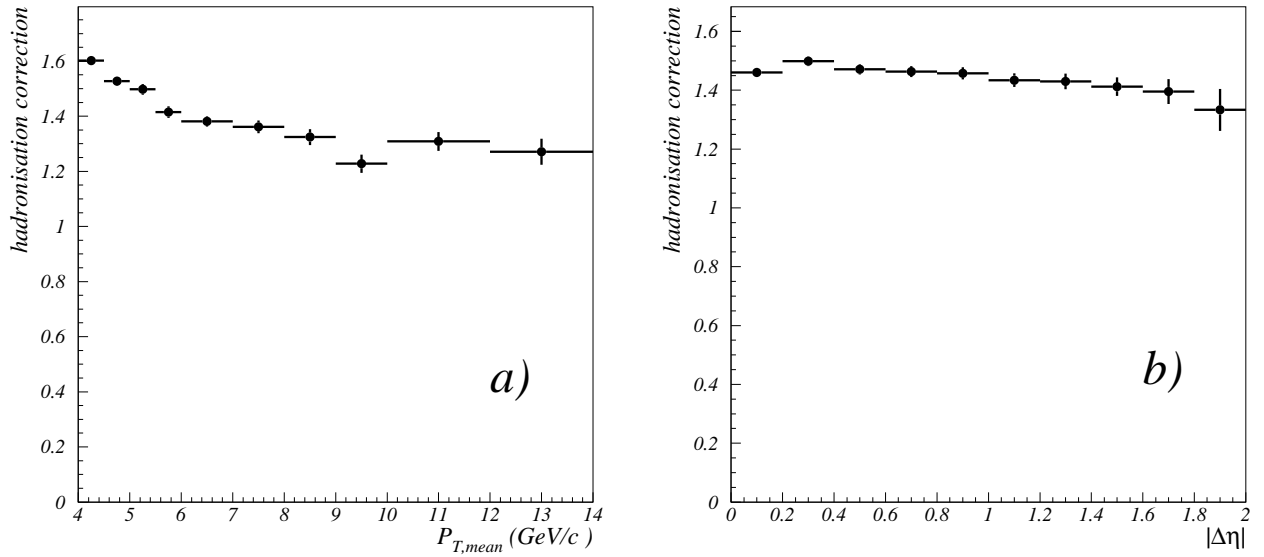


Figure 5: Hadronisation corrections as a function of the mean jet transverse momentum $\overline{p_T}$ (a) and the absolute difference of jet rapidities $|\Delta\eta|$ (b).

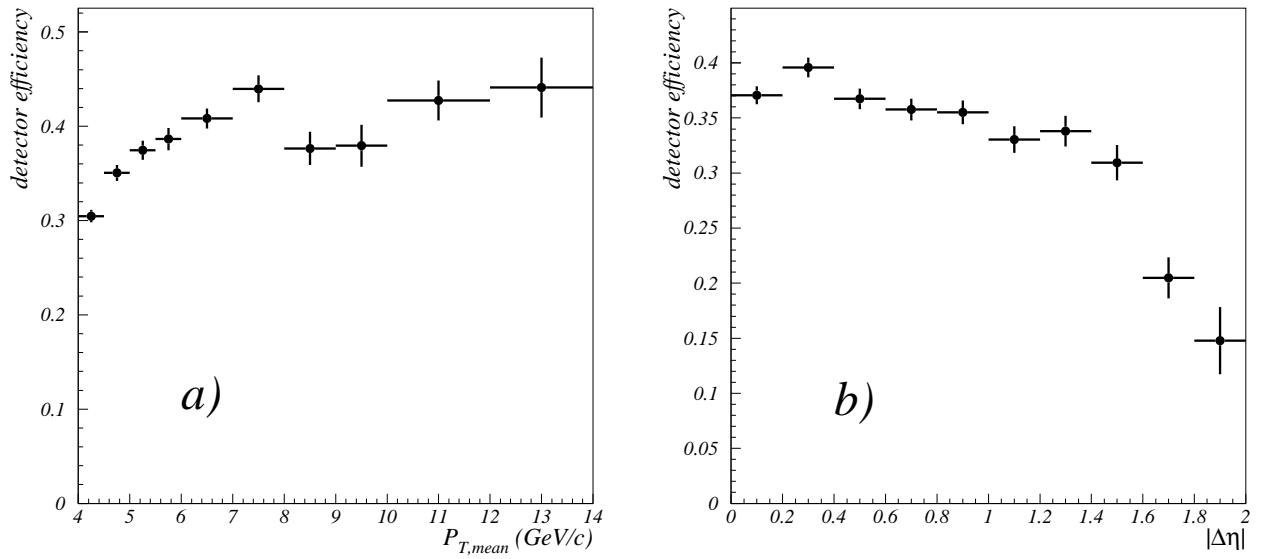


Figure 6: Detector efficiency as a function of $\overline{p_T}$ (a) and $|\Delta\eta|$ (b).

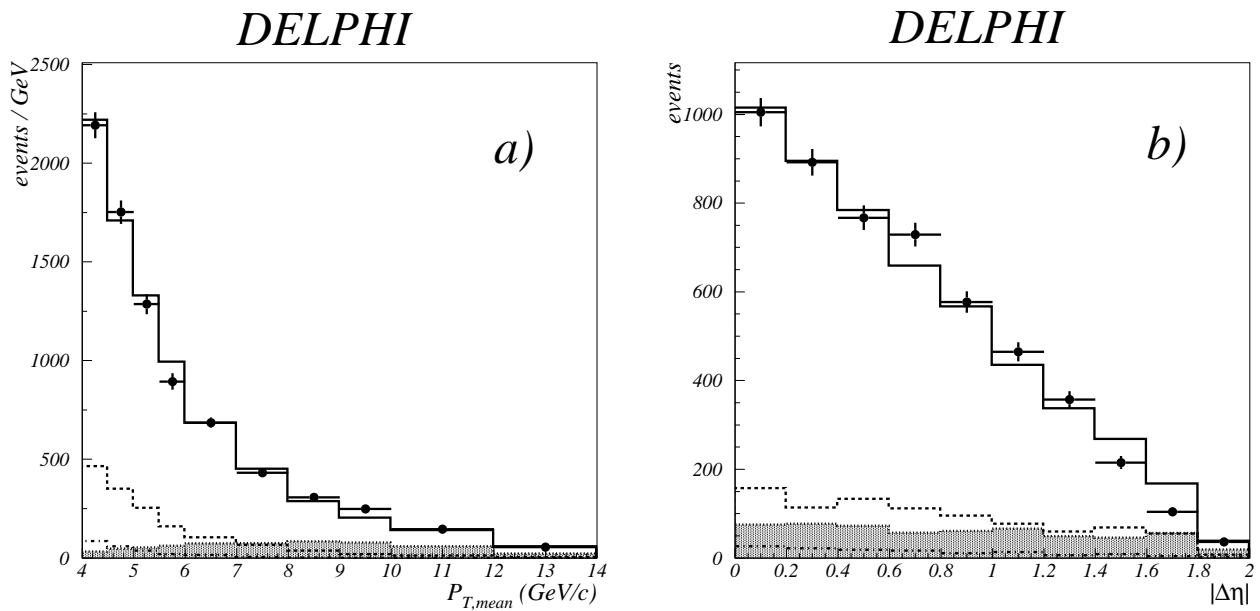


Figure 7: Distributions of the mean jet transverse momentum $\overline{p_T}$ (a) and the absolute difference of jet rapidities $|\Delta\eta|$ (b). The data are presented by bars, the sum of the scaled PYTHIA prediction and of the background by solid histograms. The background components are shown by dash-dotted lines (MIA contribution), by dashed lines ('non2-to-2 jets' background) and by shaded histograms ('non- $\gamma\gamma$ ' background).

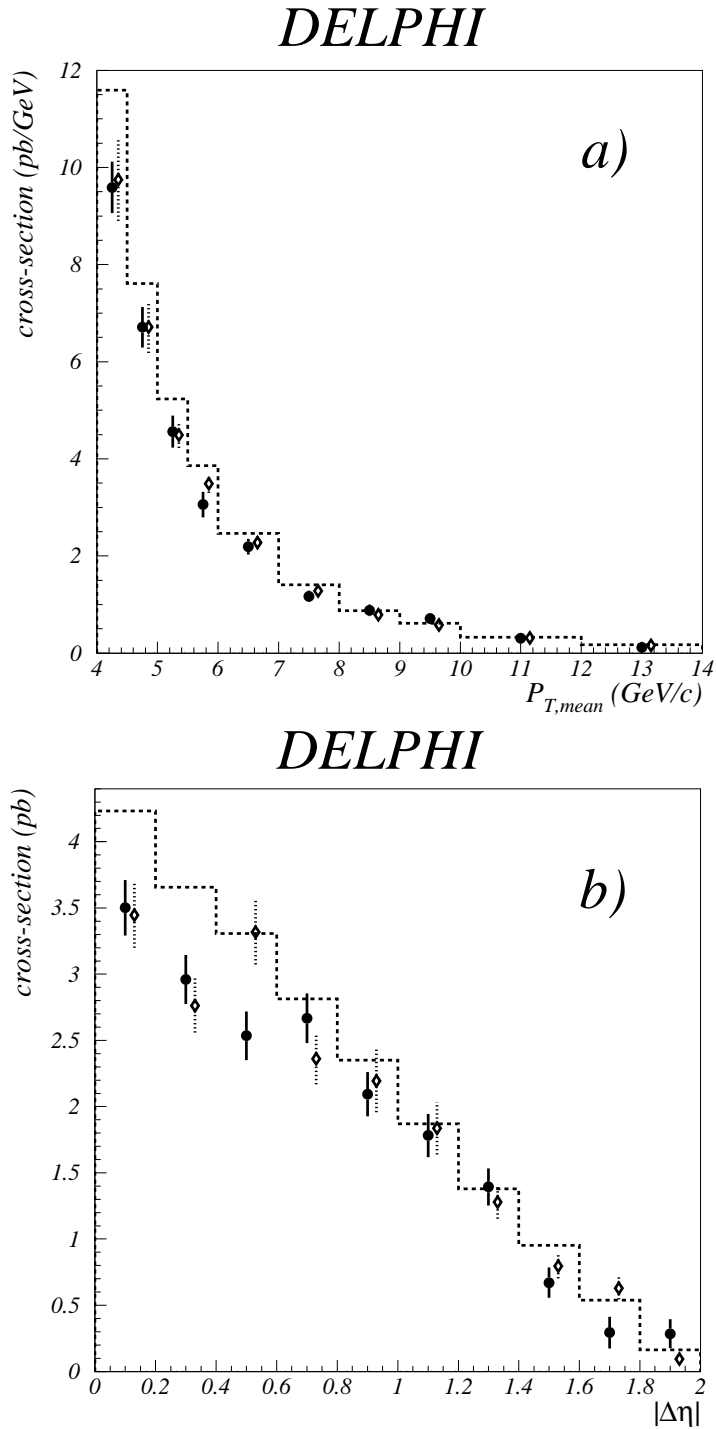


Figure 8: Cross-section of di-jet production in quasi-real $\gamma\gamma$ interactions as a function of $\overline{p_T}$ (a) and $|\Delta\eta|$ (b). The jets are reconstructed by the k_{\perp} -cluster algorithm within the pseudo-rapidity range of $-1 < \eta < 1$ and the jet transverse momentum p_T above 3 GeV/c . Dashed histograms show the leading order calculations and next-to-leading order calculations [1] are presented by open diamonds.

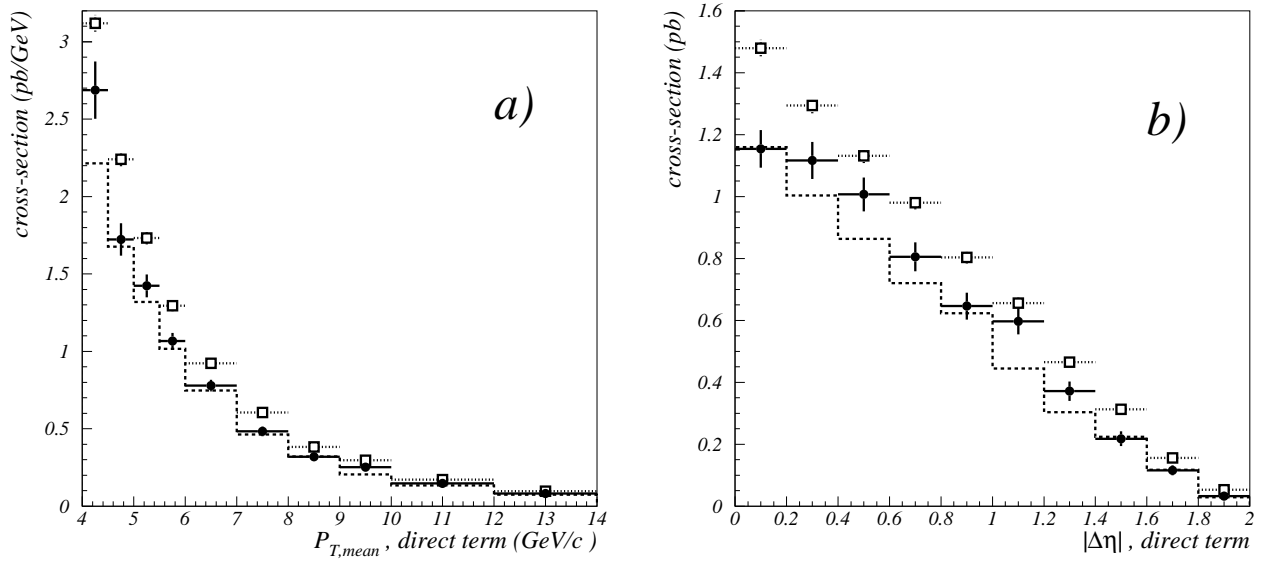


Figure 9: Cross-section of the ‘direct’ term as a function of $\overline{p_T}$ (a) and $|\Delta\eta|$ (b). Dashed histograms correspond to the PYTHIA predictions scaled according to the fit. The circles (squares) present the results of the NLO (LO) calculations [1].